High-efficiency cold-atom transport into a waveguide trap

A.P. Hilton,[1,*] C. Perrella,[1] F. Benabid,[2] B.M. Sparkes,[1] A.N. Luiten,[1] and P.S. Light[1]

[1] *Institute for Photonics and Advanced Sensing and School of Physical Sciences, The University of Adelaide, Adelaide, South Australia 5005, Australia*

[2] *GPPMM Group, Xlim Research Institute, UMR CNRS 7252, Université de Limoges, 87032 Limoges, France*

(Received 13 February 2018; revised manuscript received 14 August 2018; published 12 October 2018)

We develop and characterize an atom-guiding technique that loads 3×10^6 cold rubidium atoms into a hollow-core optical fiber, an order-of-magnitude greater than previously reported results. This result is possible because it is guided by a physically realistic simulation that can provide the specifications for a loading efficiency of 3.0% and a peak optical depth of 600. The simulation further shows that the loading efficiency is limited solely by the geometric overlap of the atom cloud and the optical guide beam, and is thus open to further improvement with experimental modification. The experimental arrangement allows observation of the real-time effects of light-assisted cold-atom collisions and background-gas collisions by tracking the dynamics of the cold-atom cloud as it falls into the fiber. The combination of these observations, and physical understanding from the simulation, allows estimation of the limits to loading cold atoms into hollow-core fibers.

DOI: 10.1103/PhysRevApplied.10.044034

I. INTRODUCTION

Cold atoms have been a transformational tool for sensing [1–3], measurement [4–8], emulation [9], and simulation [10,11]. The specific properties of cold matter that make it useful for these applications is its high atomic density, low velocity, and excellent isolation from the environment. Furthermore, alkali metals are commonly used in cold-matter experiments as they confer strong atom-light interaction, allowing both efficient measurement and manipulation. The figures of merit that quantify these properties for an atomic ensemble are its coherence time, τ, and optical depth, defined as $\mathcal{D}^{\mathrm{opt}} = -\ln T$, where T is the transmission. Examples where overall performance depends crucially on these figures of merit include quantum-state storage [1,12], strong photon-photon interaction for quantum-information processing [13], and interferometric magnetic gradiometry [14].

A promising approach to attain a high $\mathcal{D}^{\mathrm{opt}}$ is the loading of cold atoms into a hollow-core photonic crystal fiber (HC PCF) [15–17]. The tight confinement of atoms to the core of the fiber delivers a close match between the optical cross section of the cold atom and the transverse-mode diameter of the light field. The close matching leads to an optimal $\mathcal{D}^{\mathrm{opt}}$ for a given number of atoms. Further, the guidance of the fiber means the match can be extended over lengths that are not limited by diffraction—up to tens of centimeters.

Previous experiments aimed at loading cold atoms into a HC PCF achieved $\mathcal{D}^{\mathrm{opt}}$ up to 1000 [18] and were used to demonstrate slow and stopped light [19] as well as highly efficient few-photon all-optical switching [20] and excitation of Rydberg atoms [21]. Similar systems have shown coherence times not limited by atom-wall or atom-guide interactions using Lamb-Dicke spectroscopy in a one-dimensional lattice [22], or atom interferometry using optically confined free-falling cold atoms [23].

These preliminary explorations show promising results; however, the limitations and dynamics of the atomic loading and trapping process are still not well understood. This work provides a detailed simulation of the cold-atom loading of an optical fiber, which is augmented with an innovative experimental design that can follow the atoms during the loading and trapping process. The simulation is seen to be in excellent agreement with the experiment, and the imbued confidence allows rapid pinpointing of the optimal conditions in which more than 3×10^6 cold atoms can be loaded into the fiber. Using the validated simulation, we are able to predict the limits to optical depth and coherence lifetimes and suggest techniques to expand the capacity of this platform for implementation of coherent-state storage and manipulation.

II. METHODS

The experiment uses cold rubidium-85 atoms produced in a standard three-dimensional magneto-optical trap (MOT). The atoms are cooled on the $F = 3 \rightarrow F' = 4$ cycling transition of the D_2 line, and are repumped on the $F = 2 \rightarrow F' = 3$ transition of the D_1 line, shown in Fig. 1(a). We trap 1×10^8 atoms in a cloud 2 mm in

*ashby.hilton@adelaide.edu.au

diameter with a steady-state temperature of 150 μK. The ensemble temperature is reduced below 5 μK with use of $\sigma_+\sigma_-$ polarization gradient cooling (PGC) [24]. A 10-cm length of 45-μm-core-diameter kagome-lattice fiber [see Fig. 1(b)] is situated 25 mm under the MOT as shown in Fig. 1(c). This fiber has low loss between 600 and 1600 nm, and we are able to achieve a combined efficiency of guidance and coupling into the fundamental mode of more than 70% at 780 nm. After the PGC phase, an intense guide laser [25] is switched on, producing trapping forces that cause the falling atoms within the laser field to be guided toward the core of the fiber. The guide beam is coupled into the fiber from below, which produces an attractive dipole trap within the hollow-core fiber that diverges from the output to produce a conical, self-aligning optical funnel that steers atoms into the fiber. With more than 1 W of guide light detuned by 1 THz to the red of the D_1 transition, we produce a radial trapping field with a peak trap depth U_{dip} of 20 μK at the MOT location without the need for intricate magnetic field guides [26]. The eventual fraction of atoms guided into the fiber depends on the velocity and density distributions of the initial ensemble as well as its position with respect to the guide beam. These are complicated functions of the MOT and PGC parameters as well as the settings of the background-magnetic-field cancellation coils. We maximize the loading dependence on the initial state of the MOT by placing ten of the most sensitive of these variables under the control of a neural-net learning tool, M-Loop [27,28], which is capable of efficiently optimizing the in-fiber optical depth over this multidimensional space.

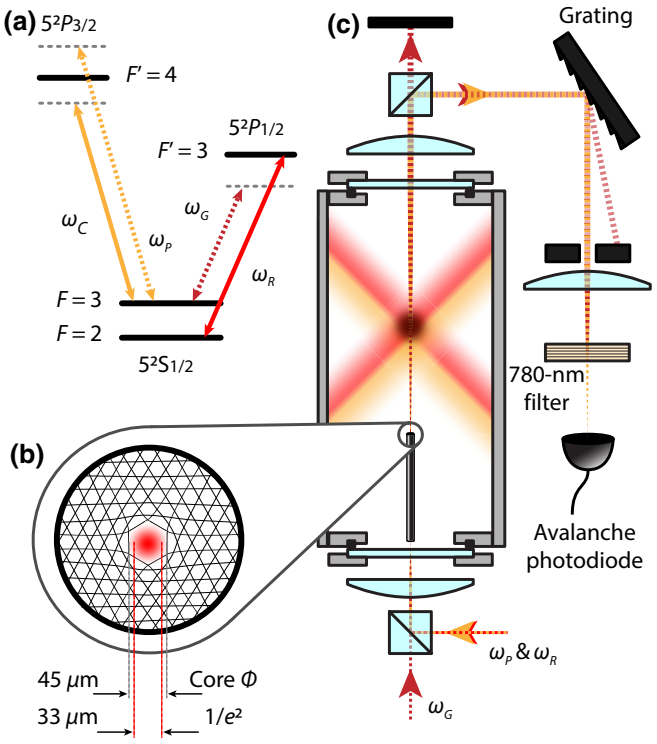

FIG. 1. Experimental setup with (a) the relevant energy levels in the D_1 and D_2 transitions, along with the relative frequency of the MOT cooling laser ω_C, the repump laser ω_R, the guide laser ω_G, and the probe laser ω_P, (b) a cross section of the kagome HC PCF, and (c) the fiber coupling system.

The number of atoms contained within the guide beam is estimated with use of the transmission of a weak (5-nW) copropagating light field that is tuned around the D_2 transition. The transmitted probe is separated from the guide with use of high-extinction polarization optics, an optical grating, and a narrow band-pass filter, which suppresses the guide light by 90 dB. Prior work [18,22,23,29] implemented a spatial-mode filter of the probe light on exit from the fiber: we do not do that here as strong lensing effects within the large fiber core [30,31] would lead to an overestimate of the optical depth.

The intense guide light introduces inhomogeneous broadening of the probe transition through its transverse intensity variation [32]. This effect is circumvented by our probing in the dark: the guide beam is rapidly intensity modulated, and probing is performed only in the absence of the guide light. We use two double-pass acousto-optic modulators in the probe path to perform the fast (30-ns) switching required. This fast switching speed provides an additional advantage in that we can step the optical frequency between each probing phase, thereby observing the full spectral width of the absorption feature over 144 MHz in a cycle lasting just 100 μs. A small amount of repump light is present with the probe, ensuring that the population is not lost to the $F = 2$ ground state during measurement. We confirm that our technique is nondestructive by applying two consecutive probe sequences and measuring less than 10% variation between measurements. During each cycle of the experiment, we probe the cold cloud with one laser pulse sequence at a predetermined time following its release from the MOT; a second identical pulse sequence is then applied 500 ms following the first. This second pulse sequence is used to normalize the cold-atom absorption as it is sufficiently delayed that it sees only a small residual absorption associated with the background of hot rubidium atoms—less than 1%.

III. ATOM-LOADING RESULTS

We compare the probe absorption when the atoms are just released from the MOT (time: 5 ms) with that observed as they just enter the fiber (time 70 ms) in Fig. 2(a). We see a peak optical depth, $\mathcal{D}^{\mathrm{opt}}$ of 600(10), comparable to the greatest depths measured in other fiber-loading experiments [18–20], and approaching the greatest depths possible with other techniques [12,33–35].

By calculating the number of atoms from $\mathcal{D}^{\mathrm{opt}}$ (see Appendix A), we estimate we have guided $3.3(1) \times 10^6$ atoms into the fiber, which is approximately 3% of the

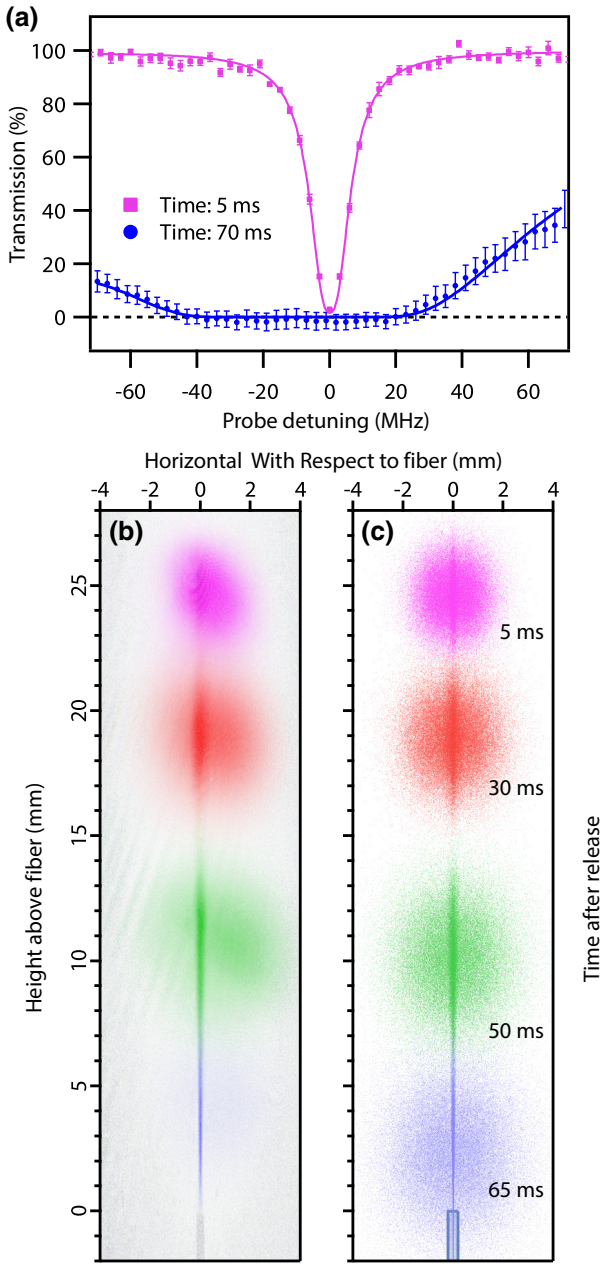

FIG. 2. Atom loading with 1 W of guide power detuned by 1 THz below the D_1 transition, with (a) transmission measurements through the fiber at 5 ms (magenta squares) and 70 ms (blue circles) with fits to data, (b) optical depth map calculated from absorption imaging from the side at 5 ms (magenta), 30 ms (red), 50 ms (green), and 65 ms (blue) after release, and (c) simulated optical depth map that matches the experimental conditions at the same instants.

MOT cloud. Using near-resonance absorption imaging from the side [see Fig. 2(b)], we can directly see the intensifying atomic density in the guide field as the atoms drop.

Because of the relatively small diffraction angle of the guide from the fiber, only 3.2% of the atoms in the initial ensemble experience a trap depth greater than the average temperature of the ensemble. The Gaussian form of the trap depth in the radial direction from the guide axis and linear scaling of trap depth with guide power impose harsh diminishing returns on atom-coupling performance for fixed cloud and trap geometries (see Appendix B). This strongly suggests that the transfer efficiency could be significantly increased by use of density-enhancing techniques in the MOT region (e.g., spatial dark spot [34,36], magnetic compression [37,38], or a vertically aligned cigar-shaped trap [39]) or by increase of the divergence of the guide by use of a smaller-core fiber.

IV. MONTE CARLO SIMULATION

The underlying physics of the atom-light interaction can be modeled with a detailed Monte Carlo simulation of the loading process. The simulation picks atoms from within a three-dimensional position and velocity distribution that is matched to the experimentally measured atom-cloud size and temperature. The evolution of the atomic position, $\mathbf{r}$, and velocity is then modeled with use of the differential equation

$$\frac{d^2\mathbf{r}}{dt^2} = -\frac{\nabla U_{\mathrm{dip}}(\mathbf{r})}{m_{\mathrm{Rb}}} + \mathbf{g}, \tag{1}$$

where m_{Rb} is the atomic mass of rubidium-85 and

$$U_{\mathrm{dip}}(\mathbf{r}) = \frac{\pi c^2}{2}\left(\frac{\Gamma_{D_1}}{{\omega_{D_1}}^3}\frac{1}{\Delta_{D_1}} + \frac{\Gamma_{D_2}}{{\omega_{D_2}}^3}\frac{2}{\Delta_{D_2}}\right) I(\mathbf{r}), \tag{2}$$

describes the potential experienced by a neutral atom in a linearly polarized dipole trap where detunings from the D_1 and D_2 transitions, Δ_{D_1} and Δ_{D_2}, are much larger than the ground-state hyperfine splitting [25] and in which the atom is subject to gravitational acceleration, $\mathbf{g} = -9.81\ \mathrm{m\,s^{-2}}\,\hat{z}$. Here Γ and ω are the decay rates and optical angular frequencies for specified transitions, and $I(\mathbf{r})$ is the local intensity of the guide beam. The simulation includes the spontaneous absorption and emission of guide photons as well as atom loss due to background-gas collisions (see Appendix C).

We are able to qualitatively test our simulation by comparing the time dynamics of the ensemble with that of the experiment. A large number (10^5) of atoms are simulated, and by calculating the position and optical depth for each atom at several time steps, we are able to replicate the data obtained experimentally using both absorption-imaging and in-fiber spectroscopy techniques. As seen in Fig. 2(c), there is excellent agreement between the experiment and the simulation. It is clear from these images that a large fraction of the initial atom cloud is not guided by the dipole trap, which highlights the importance of improving the mode overlap of the guide and the MOT.

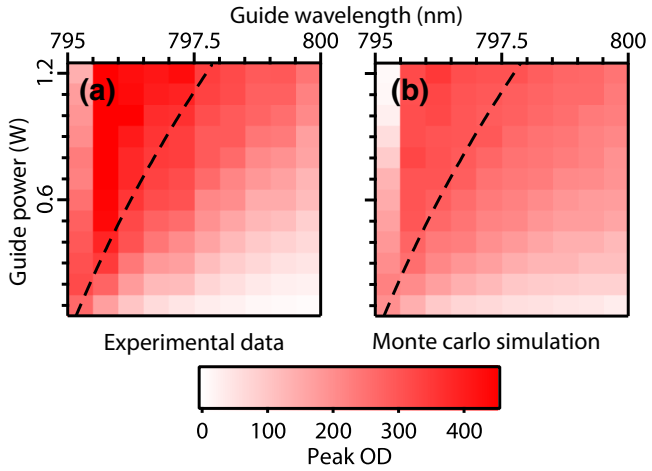

FIG. 3. Peak optical depth (OD) as a fraction of the number of atoms in the initial MOT (a) measured experimentally and (b) calculated by Monte Carlo simulation, both with the line of $U_{\mathrm{dip}} = -3\ \mu$K at the cloud (dashed black line).

We experimentally investigate the dependence of the atom-loading process on dipole-trap parameters by measuring the peak optical depth as a function of guide powers and wavelengths. These measurements, shown in Fig. 3(a), provide a quantitative means to compare the experimental results against the simulation results shown on Fig. 3(b). To ensure that the experimental atom-density distribution is a match for the assumed initial distribution in the simulation, we reduce the total atom number density by about a factor of 2 from the values shown before (since it is known that high-density MOTs have complex atomic distributions [40,41]). We see excellent agreement between experiment and simulation, both in the absolute values and in the overall shape. For conditions in which the guide is nearly resonant [the leftmost column in Fig. 3(a)], we see a reduction in the number of loaded atoms as we increase the guide depth. The simulation provides the physical understanding that this comes because of the high photon scattering rates that drive the atoms away from the fiber. We also see a plateau in the number of atoms loaded as the guide power is increased (marked by a dashed line in Fig. 3), corresponding to a trap deep enough to catch all the atoms in the volume defined by the overlap of the guide and initial atom ensemble. We note that there are no free parameters in the simulation, which emphasizes the strength of the model.

V. TIME DYNAMICS

We investigate the time dynamics of the loading process by taking absorption measurements at 4-ms intervals following the release of the MOT [similar to that shown in Fig. 2(a)]. Fitting to each spectrum with the expected line shape provides $\mathcal{D}^{\mathrm{opt}}$, and we convert this to the equivalent number of atoms in the fiber. To estimate the uncertainty of each measurement and also improve the statistics, we use five averages for each time step.

This procedure is performed in guide detuning steps of approximately 200 GHz out to 2.5 THz below the D_1 transition. We show in Fig. 4 the temporal evolution of the number of atoms for three of these different wavelengths. We note that these curves display considerably different loading behaviors. For a near-detuned guide we see a very clear peak in the number of atoms in the fiber, followed by a rapid decay, and a weak resurgence at 250 ms. For a 1.1-THz guide detuning we see a similar dramatic increase in the number of atoms at approximately 70 ms but with a much slower exponential decay of the number of atoms. For a 2.1-THz guide detuning, where one might have expected weaker interaction with the guide and thus similar behavior to the 1.1 THz result, we observe an initially higher decay rate. At longer times we see a return to an exponential decay with a similar coefficient as for the 1.1-THz detuning situation. Between these specific examples, the loading dynamics follow a smooth transition between each regime.

Our simulation allows us to explain these behaviors: for near detuning the rate of photon scattering from the guide is high and atoms are quickly expelled from the fiber, leading to the strong decay. As seen in Fig. 4, some of the atoms that have been pushed upward eventually reenter the fiber at a later time, leading to the observation of the resurgence of absorption associated with "bouncing" atoms. The theoretical treatment allows us to observe these "bouncing" atoms in the simulated absorption images [42]. For the case with 1.1-THz detuning, the scattering rate is small enough that we do not see this repulsive effect of the guide. In this case, the residual exponential loss is associated with background-gas collisions; the observed decay rate allows calculation of the residual-background-gas density within

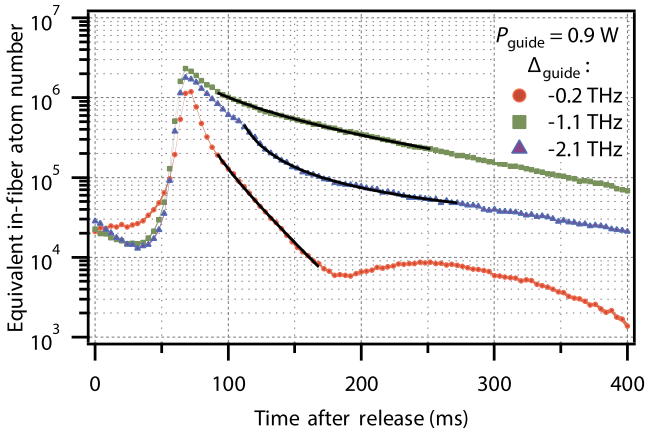

FIG. 4. Number of atoms in the fiber calculated from the optical depth at three different guide detunings. The trap depths at the cloud are 150, 22, and 13 μK for detunings of 0.2, 1.1, and 2.1 THz respectively.

the fiber (see below). For the 2.1-THz guide detuning, we believe that we are driving a photoassociation transition resulting in the formation of excited Rb_2 molecules that are lost from the trap [43]. The photoassociation rate is proportional to the density of Rb atoms and hence becomes negligible once the density has fallen sufficiently.

We fit the evolution of the number of atoms for the family of guide detunings to an equation of the form

$$\frac{dN(t)}{dt} = -\gamma N(t) - \beta'(\lambda)N(t)^2, \tag{3}$$

where γ is the loss rate due to atomic collisions, and $\beta'(\lambda)$ is the wavelength-dependent photoassociation loss coefficient, to extract a collisional loss rate γ of 7.6(2) s^{-1}. The derived density-independent loss rate has a similar value to measurements made by Osaka *et al.* [22] (2.9 s^{-1}) in a shorter section of fiber (32 mm). The background rubidium densities in the chamber and the fiber are below 1×10^{-10} Torr, which results in a Rb-Rb collision rate that is 100-fold too low to explain the observed collision-related loss [44]. We thus attribute these losses to collisions with background-gas atoms; if, as expected, this background is dominated by N_2 due to outgassing, we can calculate the background pressure from the in-fiber collision rate as $1.4(2) \times 10^{-7}$ Torr [44,45]. We can separately calculate the N_2 pressure in the chamber from the measured MOT loading time constant, giving a value of $2.0(2) \times 10^{-8}$ Torr. The N_2 pressure inside the fiber appears reasonable in light of the unfavorable vacuum geometry of the core of the fiber.

The value for $\beta'(\lambda)$ is more difficult to obtain precisely as it describes a density-squared dependent process that is dominant during the peak loading time, while there are other, strongly competing processes. We choose a fit window that contains the corner between the fast- and slow-loss processes (shown as solid black lines in Fig. 4). The fit quality is sensitive to the chosen start and end of this fitting window due to the simplicity of the two-parameter model and the complexity of the experimental system. As such, the results of this fitting, shown in Fig. 5, are intended only as a qualitative description. The form of $\beta'(\lambda)$ shows a decrease from the rapid decay experienced near resonance to a minimum at a detuning of approximately -1 THz, before smoothly increasing as the guide is detuned further. Is it possible to convert the number loss rate β' to the density loss rate β by estimation of the total volume of the atomic sample, which we calculate from the Monte Carlo simulation to be 6×10^{-6} cm^3. Using this value for the volume, we calculate $\beta(\lambda)$ to be as low as 5×10^{-11} cm^3 s^{-1} and as high as 2×10^{-9} cm^3 s^{-1}, values that are comparable to values in the literature for similarly sized dipole traps [46,47].

As the density-dependent loss term restricts the usable optical depth of the system, the ability to select a wavelength for which the coefficient is minimized is of key importance.

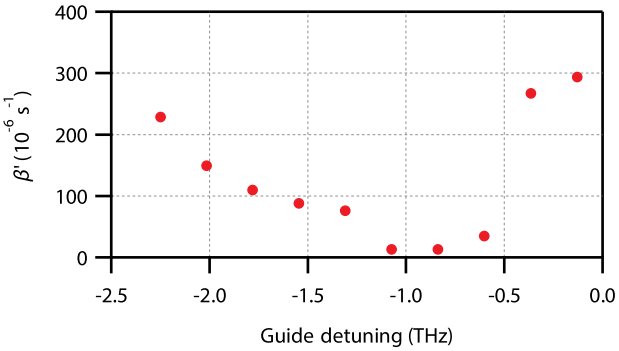

FIG. 5. Estimation of $\beta'(\lambda)$ from fits to atom-decay curves as in Fig. 4.

VI. PERFORMANCE AND LIMITATIONS

We demonstrate a highly efficient mechanism for transferring cold atoms into a waveguide. Most applications to which this extreme medium could be targeted will depend on the achievable optical depth and coherence time of the medium.

The highest optical depth attained in our system is 600(10) under typical operating conditions. The current limit to this performance is the due to the geometric mismatch between the guide beam and the MOT, with approximately 3% of the initial cloud coupled into the fiber. This fraction could be dramatically increased by use of densifying techniques such as a spatial dark spot MOT, or by change to a high-aspect-ratio cigar-shaped MOT.

We also investigate the dependence and dynamics of the loading process on wavelength and power of the guide; in this process we identify a density-dependent atom-loss term that is likely associated with photoassociation. This process can result in an unwanted reduction in the number of loaded atoms, but can be alleviated by the tuning of the guide wavelength to avoid a photoassociation transition.

The atomic coherence time will be limited by the faster of two effects: decoherence induced by interaction between trapped atoms and the optical guide field, or the loss of atoms. Photon scattering in the current experiment limits the atomic coherence time to around 200 μs, although this rate could be much reduced by replacement of the attractive guide with a hollow repulsive guide mode [48]. This trap geometry would confine atoms predominantly within the low-intensity region, vastly reducing the scattering rate. We simulate this situation, using a hollow trap of the same peak intensity as our Gaussian trap, to predict the time between photon-scattering events of 10 ms—a 100-fold improvement over the current lifetime. An alternative approach to the same end would be the use of a weak far-off-resonance red-detuned trap; this approach has

been shown to work by use of an initial ensemble with a lower temperature or by only trapping the coldest fraction of the atomic cloud [22,23]. In these weaker red- or blue-detuned traps, the background-gas collisions will set a coherent light-atom interaction limit of 130 ms; however, even this limit can likely be extended by careful baking of the fiber to reduce outgassing.

VII. CONCLUSION

We demonstrated a HC PCF cold-atom-loading technique that is capable of loading 3×10^6 atoms into the fiber—a state-of-the-art result. Aided by a robust Monte Carlo simulation, we explore the dependence of the loading efficiency on the parameters of the optical guide beam, enabling us to generate confined-atom samples with optical depths as great as 600(10). Our rapid probing technique allows us to follow the evolution of atoms in real time, and we can use this to observe the fundamental decoherence processes that apply to the approach. Our simulation allows us to show that one could maintain these great optical depths while extending the coherence time to beyond 10 ms.

ACKNOWLEDGMENTS

We thank the South Australian Government for supporting this research through the PRIF program. This research was funded by the Australian Government through the Australian Research Council (Grant No. DE12012028). B.M.S. acknowledges support from an ARC Discovery Early Career Researcher Award (Grant No. DE170100752). We thank Marcin Witkowski for his contribution to the design and construction of the scalar-magnetic-field cancellation coils.

APPENDIX A: OPTICAL DEPTH CALCULATIONS

The optical depth for a single atom in a Gaussian probe field is given by

$$\mathcal{D}^{\text{opt}}_{\text{atom}}(\Delta') = \frac{2\sigma_{D_2}}{\pi w(z)^2} e^{\frac{-2(x^2+y^2)}{w(z)^2}} \sum_{F'} \frac{S_{3,F'}}{1+4\left(\frac{\Delta'-\Delta_{3,F'}}{\Gamma}\right)^2}, \tag{A1}$$

where Δ' is the optical detuning in the atomic reference frame, σ_{D_2} is the photon scattering cross section for the interrogated transition, $w(z)$ is the local waist of the probe, $S_{3,F'}$ are the hyperfine strength factors, and $\Delta_{3,F'}$ are the optical detunings of hyperfine levels. The velocity of the atom is accounted for by our moving to the laboratory reference frame using $\Delta' = \Delta + v_z(\omega_0/c)$.

The optical depth for an ensemble of atoms can be estimated by our summing the optical depth over each atom, or equivalently, one can integrate the product of the optical depth and the atom number density $n(\rho, z)$ over the volume:

$$\mathcal{D}^{\text{opt}} = \int_0^L \int_0^{r_{\text{core}}} n(\rho,z)\mathcal{D}^{\text{opt}}_{\text{atom}} 2\pi\rho d\rho dL, \tag{A2}$$

where L and r are the length and radius of the ensemble, respectively.

One can simplify this calculation by making the assumption that an ensemble of N_{atom} atoms is uniformly populated over L, and that the radial dependence of the atom density follows a Gaussian distribution with standard deviation x_0:

$$n(\rho,z) = \begin{cases} 0, & |z| > L/2, \\ N_{\text{atom}} \dfrac{1}{L}\sqrt{\dfrac{2}{\pi x_0^2}} e^{-\rho^2/2x_0^2}, & |z| < L/2. \end{cases} \tag{A3}$$

The integration now reduces to

$$\mathcal{D}^{\text{opt}} = \eta N_{\text{atom}} \frac{2\sigma_{D_2} S_{3,4}}{\pi w_0^2}, \tag{A4}$$

for the peak optical depth on the $F = 3 \rightarrow F = 4$ hyperfine transition, where η is a coefficient that describes the level of spatial overlap between a cloud of atoms with Gaussian radial density and uniform longitudinal density, and a Gaussian intensity profile:

$$\eta = \frac{(w/2)^2}{x_0^2 + (w/2)^2}. \tag{A5}$$

APPENDIX B: ATOM-COUPLING DEPENDENCE

The atom-capture efficiency strongly depends on the initial MOT and guide geometries. A brief algebraic analysis is done to determine the scaling of efficiency with the power and size of the guide beam.

We first approximate the guide beam to be collimated through the length of the atom cloud, and we assume that the waist, w_G, is sufficiently small at the initial atom cloud location, z_0, that the cloud can be approximated as having a uniform column number density given by $\mathcal{N}$. At z_0 the trap depth in the radial direction can be described by

$$U_{\text{dip}}(\rho) = U_0(P,\lambda)\, e^{-2\rho^2/{w_G}^2}, \tag{B1}$$

where ρ is the radial coordinate, P and λ are the optical power and wavelength of the guide, and

$$U_0(P,\lambda) = U_{\text{dip}}(0), \tag{B2}$$

$$= \alpha(\lambda)\frac{2P}{\pi {w_G}^2}, \tag{B3}$$

is the peak trap depth, with wavelength dependence $\alpha(\lambda)$.

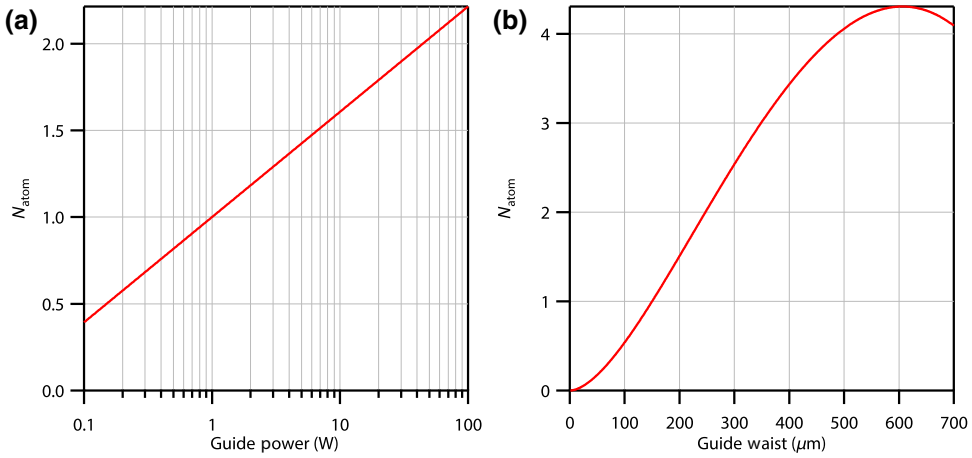

FIG. 6. Number of atoms trapped calculated with Eq. (B8), given relative to the number of atoms for U_0(797.25 nm, 1 W) and $w_G = 150$ μm, with (a) λ fixed at 797.25 nm with P varied and (b) P fixed at 1 W with w_G varied.

We consider atoms to be trapped if the trap depth at their location is greater in magnitude than the kinetic energy of the atom, and negative in sign; that is,

$$U_{\text{dip}}(\rho) + KE_{\text{atom}} < 0. \tag{B4}$$

The radius at which this is true for a fixed ensemble temperature is

$$\rho_{\text{trap}} = w_G \sqrt{\frac{1}{2} \ln\left[-\frac{U_0(P,\lambda)}{KE_{\text{atom}}}\right]}, \tag{B5}$$

and the number of trapped atoms is thus given by

$$N_{\text{atom}} = \pi \rho_{\text{trap}}{}^2 \mathcal{N}, \tag{B6}$$

$$= \frac{1}{2}\pi w_G{}^2 \mathcal{N} \ln\left[-\frac{U_0(P,\lambda)}{KE_{\text{atom}}}\right], \tag{B7}$$

$$= \frac{1}{2}\pi w_G{}^2 \mathcal{N} \ln\left[-\frac{2P\alpha(\lambda)}{\pi w_G{}^2 KE_{\text{atom}}}\right]. \tag{B8}$$

From this we can find the dependence of trapped atoms on guide power and guide waist:

$$\frac{dN_{\text{atom}}}{dP} = \mathcal{N}\frac{\pi w_G{}^2}{2P}, \tag{B9}$$

$$\frac{dN_{\text{atom}}}{dw_G} = \mathcal{N}\pi w_G \left\{\ln\left[-\frac{2P\alpha(\lambda)}{\pi w_G{}^2 KE_{\text{atom}}}\right] - 1\right\}. \tag{B10}$$

We conclude that the scaling of the number of atoms with power offers strongly diminishing returns, while increasing the divergence of the guide or the distance from the fiber to the cloud could increase the number of trapped atoms, as shown in Fig. 6.

APPENDIX C: MONTE CARLO SIMULATION

The local photon-scattering rate for an alkali-metal atom in a light field detuned from an optical transition by a distance greater than the hyperfine splitting and less than the fine splitting is given by

$$\Gamma_{\text{sc}}(\mathbf{r}) = \frac{\pi c^2 \Gamma}{2\hbar\omega_0^3}\left(\frac{1}{\Delta_{D_1}^2} + \frac{2}{\Delta_{D_2}^2}\right) I(\mathbf{r}), \tag{C1}$$

where c is the speed of light, $\hbar$ is the reduced Planck constant, w_0 is the resonance angular frequency, Δ_{D_1} and Δ_{D_2} are the detunings from the centers of the D_1 and D_2 lines, respectively, and $I(\mathbf{r})$ is the guide intensity.

We integrate $\Gamma_{\text{sc}}(\mathbf{r})$ while numerically solving the equations of motion for each atom to find the total number of scattering events up to a time t:

$$N_{\text{sc}}(t) = \int_0^t \Gamma_{\text{sc}}(\mathbf{r}(\tau))d\tau. \tag{C2}$$

Each time $N_{\text{sc}}t$ crosses an integer, we perturb the atom velocity with a kick, δv_{atom}, of

$$\delta v_{\text{atom}} = \frac{\hbar\omega_G}{m_{\text{Rb}}c}\hat{z} + \frac{\hbar\omega_{D_1}}{m_{\text{Rb}}c}\hat{\zeta}, \tag{C3}$$

where ω_G is the optical angular frequency of the guide and $\hat{\zeta}$ is a unit vector randomly generated in spherical coordinates. The first term represents a velocity kick in the direction of the guide due to spontaneous absorption, and the second term represents a velocity kick in a random direction due to spontaneous emission.

The simulation also allows for background-gas collisions by probabilistically eliminating atoms from the simulation. The probability that an atom does not experience a collision in the time frame δt is given by

$$P_c = e^{-\gamma_i \delta t}, \tag{C4}$$

where γ_i is the atom-loss rate either outside or inside of the fiber, γ_{chamber} or γ_{fiber}. By sampling of this probability

at sufficiently fine time intervals during the calculation, the population decays by the appropriate rate.

[1] M. Kasevich and S. Chu, Atomic Interferometry using Stimulated Raman Transitions, Phys. Rev. Lett. **67**, 181 (1991).

[2] I. Dutta, D. Savoie, B. Fang, B. Venon, C. L. Garrido Alzar, R. Geiger, and A. Landragin, Continuous Cold-Atom Inertial Sensor with 1 Rotation Stability, Phys. Rev. Lett. **116**, 183003 (2016).

[3] B. Canuel, F. Leduc, D. Holleville, A. Gauguet, J. Fils, A. Virdis, A. Clairon, N. Dimarcq, Ch J. Bordé, A. Landragin, and P. Bouyer, Six-Axis Inertial Sensor using Cold-Atom Interferometry, Phys. Rev. Lett. **97**, 010402 (2006).

[4] A. Peters, K. Y. Chung, and S. Chu, High-precision gravity measurements using atom interferometry, Metrologia **38**, 25 (2001).

[5] J. K. Stockton, K. Takase, and M. A. Kasevich, Absolute Geodetic Rotation Measurement Using Atom Interferometry, Phys. Rev. Lett. **107**, 133001 (2011).

[6] N. Hinkley, J. A. Sherman, N. B. Phillips, M. Schioppo, N. D. Lemke, K. Beloy, M. Pizzocaro, C. W. Oates, and A. D. Ludlow, An atomic clock with 10–18 instability, Science **341**, 1215 (2013).

[7] A. D. Cronin, J. Schmiedmayer, and D. E. Pritchard, Optics and interferometry with atoms and molecules, Rev. Mod. Phys. **81**, 1051 (2009).

[8] P. A. Altin, M. T. Johnsson, V. Negnevitsky, G. R. Dennis, R. P. Anderson, J. E. Debs, S. S. Szigeti, K. S. Hardman, S. Bennetts, G. D. McDonald, L. D. Turner, J. D. Close, and N. P. Robins, Precision atomic gravimeter based on Bragg diffraction, New. J. Phys. **15**, 1 (2013).

[9] A. W. Glaetzle, R. M. W. vanBijnen, P. Zoller, and W. Lechner, A coherent quantum annealer with Rydberg atoms, Nat. Commun. **8**, 15813 (2017).

[10] C. Gross and I. Bloch, Quantum simulations with ultracold atoms in optical lattices, Science **357**, 995 (2017).

[11] J.-C. Garreau, Quantum simulation of disordered systems with cold atoms, C. R. Phys. **18**, 31 (2017).

[12] B. M. Sparkes, J. Bernu, M. Hosseini, J. Geng, Q. Glorieux, P. A. Altin, P. K. Lam, N. P. Robins, and B. C. Buchler, Gradient echo memory in an ultra-high optical depth cold atomic ensemble, New J. Phys. **15**, 085027 (2013).

[13] Z.-Y. Liu, Y.-H. Chen, Y.-C. Chen, H.-Y. Lo, P.-J. Tsai, I. A. Yu, Y.-C. Chen, and Y.-F. Chen, Large Cross-Phase Modulations at the Few-Photon Level, Phys. Rev. Lett. **117**, 203601 (2016).

[14] K. S. Hardman, P. J. Everitt, G. D. McDonald, P. Manju, P. B. Wigley, M. A. Sooriyabandara, C. C. N. Kuhn, J. E. Debs, J. D. Close, and N. P. Robins, Simultaneous Precision Gravimetry and Magnetic Gradiometry with a Bose-Einstein Condensate: A High Precision, Quantum Sensor, Phys. Rev. Lett. **117**, 138501 (2016).

[15] R. F. Cregan, B. J. Mangan, J. C. Knight, T. A. Birks, P. St J. Russell, P. J. Roberts, and D. C. Allan, Single-mode photonic band gap guidance of light in air, Science **285**, 1537 (1999).

[16] F. Couny, F. Benabid, and P. S. Light, Large-pitch kagome-structured hollow-core photonic crystal fiber, Opt. Lett. **31**, 3574 (2006).

[17] C. Markos, J. C. Travers, A. Abdolvand, B. J. Eggleton, and O. Bang, Hybrid photonic-crystal fiber, Rev. Mod. Phys. **89**, 045003 (2017).

[18] F. Blatt, T. Halfmann, and T. Peters, One-dimensional ultracold medium of extreme optical depth, Opt. Lett. **39**, 446 (2014).

[19] F. Blatt, L. S. Simeonov, T. Halfmann, and T. Peters, Stationary light pulses and narrowband light storage in a laser-cooled ensemble loaded into a hollow-core fiber, Phys. Rev. A **94**, 043833 (2016).

[20] T. Peyronel, M. Bajcsy, S. Hofferberth, V. Balic, M. Hafezi, Q. Liang, A. Zibrov, V. Vuletic, and M. D. Lukin, Switching and counting with atomic vapors in photonic-crystal fibers, IEEE J. Sel. Top. Quantum Electron. **18**, 1747 (2012).

[21] M. Langbecker, M. Noaman, N. Kjrgaard, F. Benabid, and P. Windpassinger, Rydberg excitation of cold atoms inside a hollow-core fiber, Phys. Rev. A **96**, 041402 (2017).

[22] S. Okaba, T. Takano, F. Benabid, T. Bradley, L. Vincetti, Z. Maizelis, V. Yampol'skii, F. Nori, and H. Katori, Lamb-Dicke spectroscopy of atoms in a hollow-core photonic crystal fibre, Nat. Commun. **5**, 4096 (2014).

[23] M. Xin, W. S. Leong, Z. Chen, and S.-Y. Lan, An atom interferometer inside a hollow-core photonic crystal fiber, Sci. Adv. **4**, e1701723 (2018).

[24] J. Dalibard and C. Cohen-Tannoudji, Laser cooling below the Doppler limit by polarization gradients: Simple theoretical models, J. Opt. Soc. Am. B **6**, 2023 (1989).

[25] R. Grimm, M. Weidem"uller, and Y. Ovchinnikov, Optical dipole trap for neutral atoms, Adv. At. Mol. Opt. Phys. **42**, 95 (2000).

[26] M. Bajcsy, S. Hofferberth, T. Peyronel, V. Balic, Q. Liang, A. S. Zibrov, V. Vuletic, and M. D. Lukin, Laser-cooled atoms inside a hollow-core photonic-crystal fiber, Phys. Rev. A **83**, 063830 (2011).

[27] P. B. Wigley, P. J. Everitt, A. van den Hengel, J. W. Bastian, M. A. Sooriyabandara, G. D. McDonald, K. S. Hardman, C. D. Quinlivan, P. Manju, C. C. N. Kuhn, I. R. Petersen, A. N. Luiten, J. J. Hope, N. P. Robins, and M. R. Hush, Fast machine-learning online optimization of ultra-cold-atom experiments, Sci. Rep. **6**, 25890 (2016).

[28] M. R. Hush, M-loop: Machine-learning online optimization package, https://github.com/michaelhush/M-LOOP (2017).

[29] M. Bajcsy, S. Hofferberth, V. Balic, T. Peyronel, M. Hafezi, A. S. Zibrov, V. Vuletic, and M. D. Lukin, Efficient All-Optical Switching Using Slow Light within a Hollow Fiber, Phys. Rev. Lett. **102**, 203902 (2009).

[30] M. Noaman, M. Langbecker, and P. Windpassinger, Microlensing-induced line shapes in a single-mode cold-atom-hollow-core-fiber interface, Opt. Lett. **43**, 3925 (2018).

[31] S. Roof, K. Kemp, M. Havey, I. M. Sokolov, and D. V. Kupriyanov, Microscopic lensing by a dense, cold atomic sample, Opt. Lett. **40**, 1137 (2015).

[32] N. Davidson, H. J. Lee, C. S. Adams, M. Kasevich, and S. Chu, Long Atomic Coherence Times in an Optical Dipole Trap, Phys. Rev. Lett. **74**, 1311 (1995).

[33] Y.-F. Hsiao, P.-J. Tsai, H.-S. Chen, S.-X. Lin, C.-C. Hung, C.-H. Lee, Y.-H. Chen, Y.-F. Chen, I. A. Yu, and Y.-C. Chen, Highly Efficient Coherent Optical Memory based on Electromagnetically Induced Transparency, Phys. Rev. Lett. **120**, 183602 (2018).

[34] K. T. Kaczmarek, D. J. Saunders, M. R. Sprague, W. S. Kolthammer, A. Feizpour, P. M. Ledingham, B. Brecht, E. Poem, I. A. Walmsley, and J. Nunn, Ultrahigh and persistent optical depths of cesium in Kagomé-type hollow-core photonic crystal fibers, Opt. Lett. **40**, 5582 (2015).

[35] Y.-F. Hsiao, H.-S. Chen, P.-J. Tsai, and Y.-C. Chen, Cold atomic media with ultrahigh optical depths, Phys. Rev. A **90**, 055401 (2014).

[36] W. Ketterle, K. B. Davis, M. A. Joffe, A. Martin, and D. E. Pritchard, High Densities of Cold Atoms in a Dark Spontaneous-Force Optical Trap, Phys. Rev. Lett. **70**, 2253 (1993).

[37] M. T. Depue, S. LukmanWinoto, D. J. Han, and D. S. Weiss, Transient compression of a MOT and high intensity fluorescent imaging of optically thick clouds of atoms, Opt. Commun. **180**, 73 (2000).

[38] W. Petrich, M. H. Anderson, J. R. Ensher, and E. A. Cornell, Behavior of atoms in a compressed magneto-optical trap, J. Opt. Soc. Am. B **11**, 1332 (1994).

[39] Y.-W. Lin, H.-C. Chou, P. P. Dwivedi, Y.-C. Chen, and I. A. Yu, Using a pair of rectangular coils in the MOT for the production of cold atom clouds with large optical density, Opt. Express **16**, 3753 (2008).

[40] T. Walker, D. Sesko, and C. Wieman, Collective Behavior of Optically Trapped Neutral Atoms, Phys. Rev. Lett. **64**, 408 (1990).

[41] G. L. Gattobigio, T. Pohl, G. Labeyrie, and R. Kaiser, Scaling laws for large magneto-optical traps, Phys. Scr. **81**, 025301 (2010).

[42] See Supplemental Material at http://link.aps.org/supplemental/10.1103/PhysRevApplied.10.044034 for simulation atom-bounce absorption images.

[43] J. D. Miller, R. A. Cline, and D. J. Heinzen, Photo Association Spectrum of Ultracold Rb Atoms, Phys. Rev. Lett. **71**, 2204 (1993).

[44] U. D. Rapol, A. Wasan, and V. Natarajan, Loading of a Rb magneto-optic trap from a getter source, Phys. Rev. A **64**, 023402 (2001).

[45] T. Arpornthip, C. A. Sackett, and K. J. Hughes, Vacuum-pressure measurement using a magneto-optical trap, Phys. Rev. A **85**, 033420 (2012).

[46] S. J. M. Kuppens, K. L. Corwin, K. W. Miller, T. E. Chupp, and C. E. Wieman, Loading an optical dipole trap, Phys. Rev. A **62**, 013406 (2000).

[47] A. Fuhrmanek, R. Bourgain, Y. R. P. Sortais, and A. Browaeys, Light-assisted collisions between a few cold atoms in a microscopic dipole trap, Phys. Rev. A **85**, 062708 (2012).

[48] J. Poulin, P. S. Light, R. Kashyap, and A. N. Luiten, Optimized coupling of cold atoms into a fiber using a blue-detuned hollow-beam funnel, Phys. Rev. A **84**, 053812 (2011).